

Observations of rotational magnetic moments in the ground and some excited vibrational Σ states of C_2H_2 , C_2HD , and C_2D_2 by magnetic vibrational circular dichroism

Cheok N. Tam

Department of Chemistry, University of Illinois at Chicago, M/C 111, 845 West Taylor Street, Chicago, Illinois 60607-7061

Petr Bour

Department of Chemistry, University of Illinois at Chicago, M/C 111, 845 West Taylor Street, Chicago, Illinois 60607-7061 and Institute of Organic Chemistry and Biochemistry, Academy of Sciences of the Czech Republic, Flemingovo nam. 2, 16610, Praha 6, Czechoslovakia

Timothy A. Keiderling

Department of Chemistry, University of Illinois at Chicago, M/C 111, 845 West Taylor Street, Chicago, Illinois 60607-7061

(Received 28 August 1995; accepted 18 October 1995)

Magnetic vibrational circular dichroism (MVCD) spectra of acetylene and its deuterated isotopomers have been recorded for the following Σ symmetry combination and overtone bands of C_2H_2 : $\nu_4 + \nu_5$; C_2HD : $\nu_4 + \nu_5$, $2\nu_4$, $2\nu_5$; C_2D_2 : $\nu_4 + \nu_5$, the ν_3 fundamental for C_2HD and C_2D_2 ; and the $\nu_4 \rightarrow 2\nu_4 + \nu_5$ and $\nu_5 \rightarrow \nu_4 + 2\nu_5$ hot bands for C_2H_2 . For a $\Sigma_g \rightarrow \Sigma_u$ transition, the MVCD A terms observed must arise primarily from the rotational Zeeman effect. These negative A_1/D_0 values for low J'' transitions confirm that the sign of the rotational g -value for acetylene is *positive*. The rotational magnetic moments in both the lower and upper vibrational states were determined by comparison of moment analyses of experimental and simulated MVCD spectra obtained with a model Hamiltonian for acetylene. The g_J values in all the excited bending combination and overtone vibrational levels observed are smaller than those in the ground and the first excited stretching vibrational levels. This observation has been confirmed by theoretical simulation of the MVCD spectra of the $\nu_4 + \nu_5$ combination band of C_2H_2 . From these MVCD results, for C_2H_2 , $g_J(\text{ground}) = +0.0535 \pm 0.0033$ and $\Delta g(\nu_4 + \nu_5) = -0.0061 \pm 0.0004$; for C_2D_2 , $g_J(\text{ground}) \sim g_J(\nu_3) = +0.0363 \pm 0.0048$, $\Delta g(\nu_4 + \nu_5) = -0.0052 \pm 0.0031$; and for C_2HD , $g_J(\text{ground}) \sim g_J(\nu_3) = +0.0409 \pm 0.0069$. These are the first quantitative, MVCD determinations of nondegenerate excited state g values distinctly different from the ground state. The decrease in g value correlates with off-axis deformation of the linear C_2H_2 rotation. © 1996 American Institute of Physics. [S0021-9606(96)01704-5]

I. INTRODUCTION

Acetylene, C_2H_2 , is a linear polyatomic molecule in the ground electronic state. It has seven vibrational modes of which two bending modes are degenerate.¹ The whole infrared spectrum of acetylene has been extensively studied at high resolution resulting in determination of accurate molecular constants.²⁻⁵ Besides the fundamental vibrational bands, the infrared spectrum of acetylene also contains several combination bands and hot bands with considerable intensity.²⁻⁵ In particular in the IR, the $\Sigma_u^+(\nu_4 + \nu_5)$ combination band has roughly the same intensity as the fundamental $\Sigma_u^+(\nu_3)$ out of phase C-H stretching band.

Molecular Zeeman studies of acetylene are less developed and have a somewhat controversial history. Acetylene cannot be studied by microwave spectroscopy due to its lack of a permanent dipole moment. The rotational g_J value in the ground vibrational state was first measured by Ramsey and co-workers and was determined to be *negative* (-0.04903 ± 0.00004) using the molecular beam magnetic resonance (MBMR) technique.⁶ However, measurements of transverse heat flow in C_2H_2 under the influence of a magnetic field and

molecular Zeeman studies of molecules related to acetylene,⁷ were found to be consistent with a *positive* g_J value of that magnitude. Subsequently, Ramsey and co-workers corrected their earlier mistake using a revised experimental procedure and agreed that the sign of the g_J value for C_2H_2 should be *positive*.⁸ Recently, We have reconfirmed, independently of MBMR methods, that the correct sign of this g_J value is unambiguously *positive* by using magnetic vibrational circular dichroism (MVCD).⁹

MVCD is the differential absorption of left and right circular polarized light by vibrational transitions of molecules in the presence of an external magnetic field parallel to the propagation direction of the light. MVCD was first observed¹⁰ and applied in the studies of molecules with high symmetries in the condensed phase.¹¹⁻¹³ Recently, MVCD has been extended to studies of the molecular Zeeman effect of small molecules in the gas phase.^{14,15} The MVCD method of determining the molecular Zeeman effect has been "calibrated" by the determination of the rotational g_J value of $C \equiv O$ and $H(D)Cl$ and comparison to literature values.^{16,17} These molecular Zeeman studies showed that MVCD is

trivially able to determine the sign of the rotational g_J value for most transitions and can approximately measure its magnitude (to roughly an accuracy of $\pm 10\%$) by use of a relatively simple experimental setup.

Since MVCD is an intensity measurement, it will never have the quantitative precision of the conventional frequency based techniques as regards the magnitude of the g value. The advantage of MVCD derives from its high sensitivity, through which Zeeman splittings that are roughly three orders of magnitude smaller than our current limiting resolution can be sensed. Furthermore, since ro-vibrational transitions are measured, MVCD actually samples the Zeeman properties of both the lower and upper vibrational states at the same time. We have shown, through detailed analyses of the DCI and NH_3 MVCD spectra using simulation techniques, that the overall rotational envelope of the MVCD band can be used to determine the relative g values between the ground and excited vibrational states if the change is greater than $\sim 10\%$.¹⁸

There were two major goals for our original molecular Zeeman studies of acetylene and its deuterated isotopomers. The first was to provide a direct measurement of the sign of the g_J value for unambiguous reconfirmation of the correct sign of the g_J value for acetylene. This has already been directly addressed in our preliminary report which focused only on the $P(J''=1)$ transition of the $\nu_4 + \nu_5$ combination band of C_2H_2 .⁹ Second, measurement of the rotational Zeeman effect and assessment its variation among the MVCD accessible vibrational excited states of C_2H_2 , C_2HD and C_2D_2 was sought. This paper focuses on the latter goal and presents MVCD measurements for acetylene at a nominal spectral resolution of 0.1 cm^{-1} along with moment analysis results for each of the spectrally isolated rovibrational transitions in the following Σ_u^+ (or Σ^+ for C_2HD) vibrational bands: the ν_3 C-H stretch in C_2HD and C_2D_2 ; the $\nu_4 + \nu_5$ bending combination in C_2H_2 , C_2D_2 and C_2HD ; and the $2\nu_4$ and $2\nu_5$ overtones in C_2HD . In addition, MVCD for some related hot band ($\pi_g \rightarrow \pi_u$) transitions in C_2H_2 , $\nu_4 \rightarrow 2\nu_4 + \nu_5$ and $\nu_5 \rightarrow \nu_4 + 2\nu_5$, that have no net angular momentum change are also observed. The rotational g_J values in the ground, excited bending and excited stretching vibrational levels are compared. In addition, the theoretical simulation of the IR absorption and MVCD spectra of the $\nu_4 + \nu_5$ combination band of acetylene are presented and compared to the experimental results. These latter results are the first clear demonstration of the capability of MVCD to determine excited state g values not previously available from conventional techniques. For the $\nu_4 + \nu_5$ band, the excited state g value is shown to differ from the ground state parameter and reflects geometry changes occurring with vibrational excitation of this bending combination mode in this molecule of fundamental importance.

II. EXPERIMENT

The MVCD spectra were measured using a polarization modulation instrument, based on a Digilab (BIORAD) FTS-60A FTIR with the sample placed in the bore of a 8 Tesla

superconducting magnet (Oxford Instruments). The details of this instrument have been discussed previously.¹⁹⁻²¹ The only recent modification in this instrument is the upgrade of the interferometer to the FTS-60A to allow dynamic alignment, 0.1 cm^{-1} resolution and step scan.^{22,23} The improvement in resolution from our previous measurements at 0.5 cm^{-1} ,¹⁶ resulted in enhanced signal levels and allowed better isolation of the ro-vibrational bands. Co-incidentally, this constitutes one of the first reports of MVCD (or VCD) at 0.1 cm^{-1} resolution. Two different polarization modulation optical setups were used for different spectral regions. For the spectral region from 800 to 1600 cm^{-1} , circularly polarized light is generated by a 42 mm diameter grid polarizer on a BaF_2 substrate (Cambridge Physical Sciences) in combination with a ZnSe photoelastic modulator (Hinds International). The beam transmitted by the sample is then focused onto a cooled narrow band $\text{Hg}(\text{Cd})\text{Te}$ detector (Infrared Associates) by a ZnSe lens. For spectral frequencies higher than 1600 cm^{-1} , a CaF_2 photoelastic modulator and focusing lens were substituted for the ZnSe optical components.

The experiments reported here followed general procedures used for MVCD experiments described in our previous reports.^{14,16,17,24} The normal Fourier modulation (0–4 kHz) is conventionally processed to a single beam response spectrum while the signals at the modulator frequency are demodulated through a lock-in amplifier (PAR 124A) tuned to that frequency and then fed back into the FTIR electronics. After co-addition of many scans and conversion of the resulting interferogram, a polarization modulation response spectrum is obtained. The zero path difference for this differential interferogram was determined with the aid of a fiducial mark created with a second detector signal as detailed separately.²⁰ The ratio of these spectra plus proper phase correction and intensity calibration¹⁹ produces the final MVCD spectrum.

C_2H_2 was obtained from AGA Gas, Inc (as a mixture of acetylene and acetone) and was further purified in a glass vacuum system by trapping out the acetone with a dry ice bath. No residual features for acetone were observed in the IR absorption spectra we have measured for acetylene. C_2HD was purchased from Cambridge Isotope Laboratories, Inc. and used without further purification. Since the C_2HD sample contained a considerable amount of C_2H_2 and C_2D_2 isotopic impurities, measuring the MVCD spectrum of C_2HD over a wide spectral region also gave the MVCD spectrum of C_2D_2 (with some spectral overlap) as a bonus. The samples were transferred at room temperature into a brass cell at a pressure of ~ 5 and 10 torr for C_2H_2 and C_2HD , respectively. Since the pressure broadening is of the order of 10 MHz/torr,²⁵ these pressures will not affect our detectable linewidths. This cell was sealed with two KBr windows separated by 6.2 cm and tilted by 5° from parallel, to suppress reflective multipass interference between the windows which can degrade the baseline. The frequencies and assignments for all the measured ro-vibrational transitions matched, within our measurement accuracy, those available for C_2H_2 ,⁴ C_2HD ,²⁶ and C_2D_2 ²⁷ in the literature.

MVCD spectra were scanned in both positive and nega-

tive fields, ± 8 T, to eliminate artifacts and improve the signal-to-noise ratio (S/N). Spectra were obtained as an average of 8 blocks (4 blocks for each direction of the magnetic field) of 1024 rapid scans (moving mirror speed of 0.6 cm/s). Both the infrared absorption and MVCD spectra were measured at a nominal resolution of 0.1 cm^{-1} which was subsequently degraded by triangular apodization to minimize the side bands. The resulting final full widths at half height (FWHH) for the absorbance bands around 1200 and 2500 cm^{-1} were 0.14 and 0.20 cm^{-1} , respectively. The broader linewidths in the near-IR region are probably due to beam divergence degradation of the interferogram quality in the near-IR. The phase corrected and calibrated MVCD spectra were further corrected for the field profile over the sample cell and were normalized to 1 T for presentation and analysis.

III. THEORY

To simulate the $\nu_4 + \nu_5$ combination band MVCD, a modified Wang transformed basis set was used for the rovibrational wave functions of acetylene following Herman *et al.*,²⁸ but explicitly including M , the projection of the total angular momentum J onto the magnetic field direction:

$$\begin{aligned} |e\rangle &= (2)^{-1/2}(|l_4 l_5 JM\rangle + |-l_4 - l_5 JM\rangle) \\ &= (2)^{-1/2}(|l_4 l_5\rangle + |-l_4 - l_5\rangle)|JlM\rangle, \end{aligned} \quad (1)$$

where l_4 and l_5 are the projection of the vibrational angular momenta on the $\text{C}\equiv\text{C}$ axis for the ν_4 and ν_5 mode, respectively, and l is the total vibrational momentum (equal to the projection of J onto the molecular axis $\text{C}\equiv\text{C}$). The usual parity labeling is used,²⁸ with the Watson phase convention.²⁹ An electric dipolar transition to the corresponding f functions,

$$|f\rangle = (2)^{-1/2}(|l_4 l_5\rangle - |-l_4 - l_5\rangle)|JlM\rangle, \quad (2)$$

is not allowed for the P and R branches. Thus for the ground state, $l_4=0$, $l_5=0$, $l=0$, and the wave function is simply represented as:

$$|0\rangle = |JlM\rangle = |J0M\rangle, \quad (3)$$

while for the Σ_u^+ ($\nu_4 + \nu_5$) excited state a 2×2 matrix spanned by the two possible vibrationally symmetric ($|e\rangle$ type) wave functions

$$|1\rangle = (2)^{-1/2}(|11\rangle + |-1 - 1\rangle)|J2M\rangle \quad (4a)$$

and

$$|2\rangle = (2)^{-1/2}(|1 - 1\rangle + |-11\rangle)|J0M\rangle. \quad (4b)$$

must be diagonalized to get the proper rovibrational eigenfunctions.

The Hamiltonian for constructing this matrix without an external field is known and was described previously.^{28,30} Pliva's parametrization was used for the interaction Hamiltonian in the absence of an applied field.³ For simulation of the molecular Zeeman effect, we add the first-order perturbations to the diagonal elements caused by the magnetic field, \mathbf{B} . Thus the new diagonal matrix elements are

$$H'_{11} = H_{11} - g_{J2} \mu_N M B \quad (5a)$$

and

$$H'_{22} = H_{22} - g_{J0} \mu_N M B, \quad (5b)$$

where μ_N is the nuclear magneton and g_{JI} the molecular g value. There are no off-diagonal Zeeman terms since our basis functions are diagonal in the Zeeman operator.

The molecular magnetic moment, \mathbf{m} , is a vector sum of the vibrational and rotational moments and can be expressed as

$$\mathbf{m} = (g_v \mathbf{I} + g_R \mathbf{R}) \mu_N. \quad (6)$$

Because only the projection, m_J of the total angular momentum, \mathbf{J} , is conserved, we can write,

$$\begin{aligned} m_J &= \mathbf{m} \cdot \frac{\mathbf{J}}{|\mathbf{J}|} = \frac{g_v \mathbf{I} \cdot \mathbf{J} + g_R (\mathbf{J} - \mathbf{I}) \cdot \mathbf{J}}{|\mathbf{J}|} \mu_N \\ &= \frac{(g_v - g_R) l^2 + g_R J(J+1)}{[J(J+1)]^{1/2}} \mu_N. \end{aligned} \quad (7)$$

Reformulating m_J in terms of a molecular g value, g_{JI} , yields

$$m_J = g_{JI} \mu_N |\mathbf{J}|, \quad (8)$$

which combined with Eq. (7) can be used to relate the apparent g value, g_{JI} , with the vibrational and rotational g values, g_v and g_R , respectively as

$$g_{JI} = g_R + (g_v - g_R) \{l^2 / [J(J+1)]\}. \quad (9)$$

It might be noted that in the absence of a vibration-rotation interaction, only $|2\rangle$ [Eq. (4)] would give rise to observable ro-vibrational transitions. Since the vibrational mode symmetry is Σ_u^+ for most of the allowed excited states considered here, the vibrational g value is zero for the pure $|2\rangle$ states. After a diagonalization, two excited states are obtained as

$$|\Sigma_u^+ JM\rangle = C_1^\sigma |1\rangle + C_2^\sigma |2\rangle \quad \text{and} \quad |\Delta_u JM\rangle = C_1^\delta |1\rangle + C_2^\delta |2\rangle. \quad (10)$$

The molecular frame symmetry representations, Σ_u^+ and Δ_u , are reasonable approximations for the vibrational wavefunctions at low J only ($J < 30$).²⁸ Similarly, at low J , the experimentally observed g value must be dominated by g_R since $l=0$ then dominates our eigenfunctions for the Σ_u^+ state, i.e., $C_2^\sigma \sim 1$.²⁸ For higher J , the g value for the excited state converges relatively quickly to g_R since l is limited to 0 or 2 [Eq. (9)]. Therefore, even for the more complex states resulting from diagonalizing the interaction Hamiltonian, $g_{JI} \sim g_R$.

Fundamental formulas for the rotationally resolved MVCD have been derived recently.¹⁸ The absorption intensity for the left and right circularly polarized light (A^- and A^+ , respectively) under a transition from the ground state, $|0J''M''\rangle$ to the excited state, $|\Sigma_u^+ J'M'\rangle$, are equal to

$$\begin{aligned} A_{\pm}^{J'M'} &= \kappa \omega |C_2^\sigma|^2 \mu^2 g_{JI} |\langle 10J''0 | J'0 \rangle|^2 \\ &\quad \times |\langle 1 \pm 1 J'M' | J''M'' \rangle|^2 \exp(-\epsilon_{J''M''} / kT), \end{aligned} \quad (11)$$

where κ is a constant independent of the state, ω is the frequency of the incident light, μ is the vibrational transition moment, g_J is the nuclear statistics factor, which in this case is $g_J=1$ for even and $g_J=3$ for odd J levels. The usual notation is used for the Clebsch–Gordan coefficients; k is the Boltzman factor, T is the temperature and $\epsilon_{J''M''}$ is the energy of the rotational component of the ground state from which the transition initiates. Equation (11) is sufficient to simulate the absorption and MVCD spectra when one associates the contribution from each allowed $J'M'$ transition with a reasonable line shape and overlaps all the transition line shapes placed at their appropriate frequencies.

Alternatively, expressions for use in conventional MVCD analyses can be obtained by substituting the molecular Zeeman operator and the ro-vibrational states $|v, J, M_J\rangle$ into Stephens conventional MCD formulae³¹ for the A -term coefficient (A_1) and the dipole strength (D_0) for the overlapping $\Delta M = M \pm 1$ transitions. Because of the small magnitude of the Zeeman splitting for diamagnetic molecules, as compared to the experimental resolution used, the $J'' \rightarrow J'$ transition bandshape seen in our MVCD experiments averages over the M quantum numbers. If one assumes that the g value is independent of rotational and vibrational quantum numbers, $g_{v'} = g_{v''}$, then a simple expression for A_1/D_0 results,

$$g_{\text{eff}} = \frac{1}{2} \left(-\frac{\beta}{\mu_N} \right) \left(\frac{A_1}{D_0} \right), \quad (12)$$

where g_{eff} is the effective rotational g value, $g_{\text{eff}} = g_{v'} = g_{v''}$ in this case. The assumption that $g_{v'} = g_{v''}$, and thus is a constant, is justified for diatomics such as CO, HCl, and DCI;^{16–18} but if, on the contrary, an excited state g value is substantially different from the ground state g value, g_{eff} will not be constant.¹⁸

In general, if $g_{v''}$ and $g_{v'}$, the rotational g values for the ground and excited vibrational states respectively, are not equal, their difference may be defined as,

$$\Delta g = g_{v'} - g_{v''}. \quad (13)$$

We are interested in utilizing the results of the previously described^{16,17} moment analyses of the MVCD and absorption bands to determine $g_{v'}$ and $g_{v''}$. Using the formulae for the absorption intensities for the left and right circularly polarized light,¹⁸ the following expressions result,

$$g_{\text{eff}} = g_{v'} + \Delta g \frac{J''}{2}, \quad \text{for } J' = J'' + 1, R \text{ branch}; \quad (14a)$$

$$g_{\text{eff}} = g_{v'} - \frac{\Delta g}{2}, \quad \text{for } J' = J'', Q \text{ branch}; \quad (14b)$$

$$g_{\text{eff}} = g_{v'} - \Delta g \frac{J'' + 1}{2}, \quad \text{for } J' = J'' - 1, P \text{ branch}. \quad (14c)$$

From Eq. (14a)–(14c), it can be seen that if the g values for the ground and excited vibrational states are different, the effective g value, g_{eff} , in the P and R branches will be linearly dependent on the J'' value with a slope of $\Delta g/2$.

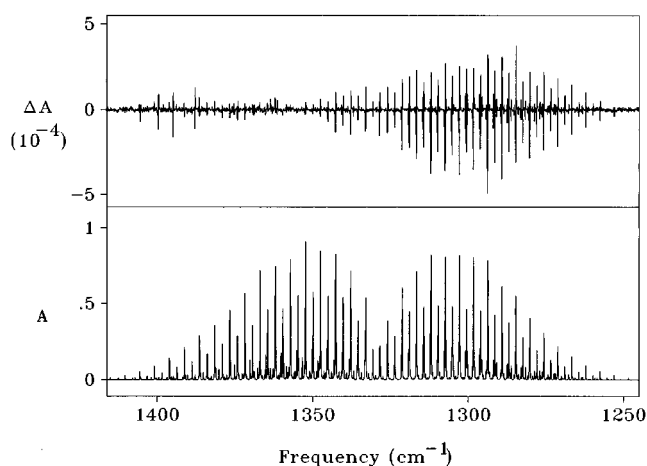


FIG. 1. The MVCD (upper) and IR absorption spectra (lower) of the $\nu_4 + \nu_5$ combination band of C_2H_2 . Resolution: 0.1 cm^{-1} MVCD shown is the difference of the MVCD measured in a field of $\pm 8 \text{ T}$, normalized to 1.0 T, each averaged over four blocks of 1024 scans.

IV. RESULTS

A. C_2H_2

Figure 1 shows the IR absorption and MVCD spectra of C_2H_2 in the mid-IR region. Figure 2(a) and 2(b) show expanded sections from Fig. 1 corresponding to high J'' values in the P and R branch, respectively, so that the contributions to the MVCD spectrum from the hot bands, $\nu_4 \rightarrow 2\nu_4 + \nu_5$ and $\nu_5 \rightarrow \nu_4 + 2\nu_5$, can be identified in the P branch. The $\nu_4 + \nu_5$ combination band has the highest intensity in this spectral region while several other hot bands and combination bands contribute smaller features. Since ro-vibrational transitions were measured at 0.1 cm^{-1} resolution, any hyperfine structure present was not resolved.

There is a large intensity difference between the clear negative A terms characteristic of the P -branch transitions and the weak R -branch transitions for the MVCD of this $\nu_4 + \nu_5$ combination band. At about the $R(J'' = 11)$ transition, the observable MVCD signal intensity collapses below the detectable limit, but at much higher J'' values in the R branch, it reappears with the opposite sign pattern, as a weak positive A term. The low S/N in Fig. 2(b) reflects the very low MVCD magnitude in this region; as such, the vertical scale divisions used are ~ 10 times smaller. In addition, there appear to be several relatively large MVCD features at the very high J'' end of the R branch [marked by # in Fig. 2(b)] which correspond to very weak absorbance features. These are due to residual water vapor inside our spectrometer. While not normally desirable, these MVCD H_2O signals provide an internal reference against which the absolute sign of the MVCD spectrum being measured can be calibrated. The overall intensity variation in the rotational envelope of the $\nu_4 + \nu_5$ MVCD suggests that the g_J value in this excited vibrational state differs from the g_J value in the ground vibrational state in a manner suggested by Eq. (14).¹⁸

For the P branch, the negative A terms which indicate a first-order Zeeman effect³¹ that would arise from a positive rotational g_J value.^{14,16,17,24} The flipped sign pattern in the

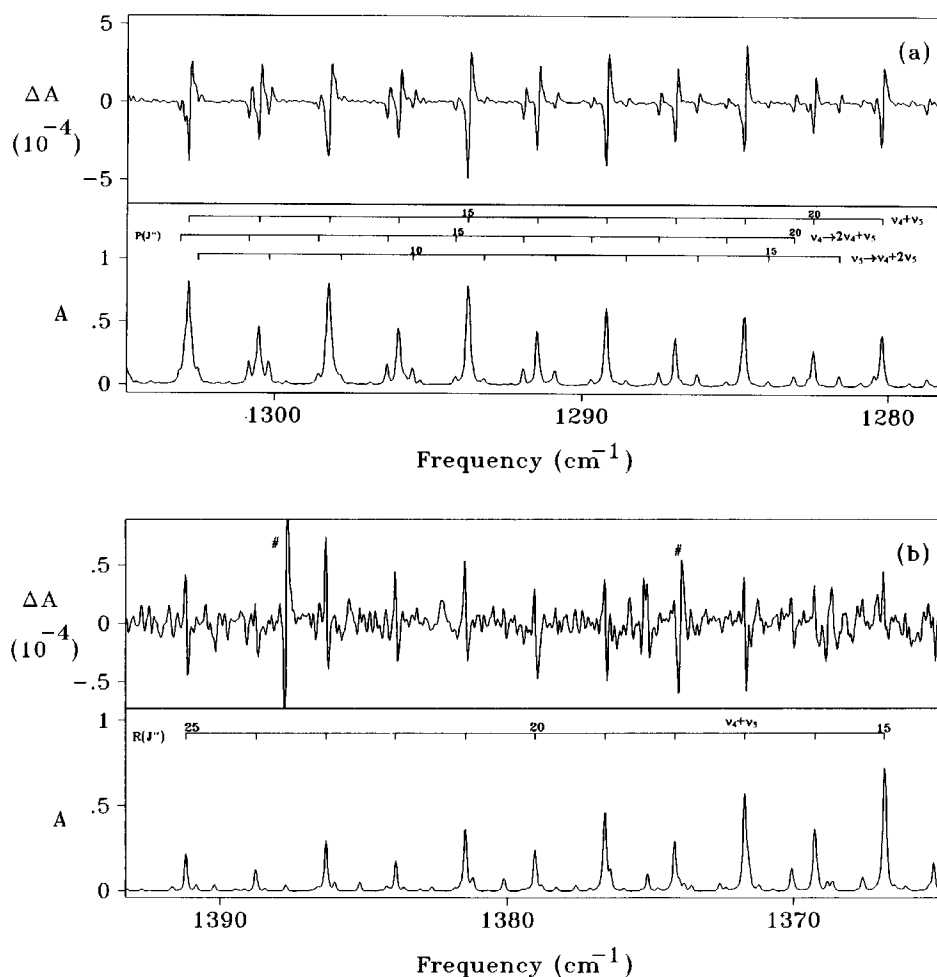


FIG. 2. (a) Part of the P branch of the MVCD (upper) and IR absorption spectra (lower) of the $\nu_4 + \nu_5$ combination band of C_2H_2 shown in Fig. 1. The two observable hot band transitions, $\nu_4 \rightarrow 2\nu_4 + \nu_5$ and $\nu_5 \rightarrow \nu_4 + 2\nu_5$ are also assigned. (b) Part of the corresponding R branch. # indicates transitions from residual H_2O vapor in our spectrometer. No observable MVCD signals for the two hot bands are identified in this R branch.

high J'' region in the R branch indicates that the effective g_J value is negative there. At very low J'' , the effective g value is positive in the region where it should most closely reflect the rotational g -value [Eq. (14)].^{18,23} Besides the $\nu_4 + \nu_5$ combination band, negative A terms for the two hot bands [$\nu_4 \rightarrow 2\nu_4 + \nu_5$ and $\nu_5 \rightarrow \nu_4 + 2\nu_5$, as assigned in Fig. 2(a)] have also been observed in part of the P branch where they happen to be well resolved, indicating a consistency in the sign of the rotational g -value sign for these transitions.

The ν_4 and ν_5 fundamentals for C_2H_2 are degenerate (π_g and π_u , respectively) and fall in a frequency region (500 – 800 cm^{-1}) which is below the normal working range of our MVCD spectrometer as configured for these experiments.²² Our preliminary results for the ν_5 mode will be discussed separately.³² The ν_3 fundamental is at about 3300 cm^{-1} where the response of our spectrometer is low when operated in the rapid scan mode used for these experiments. In that region, we have been able to obtain only very low S/N spectra which has made any reliable analysis of the ν_3 fundamental MVCD impossible.

B. C_2D_2

The MVCD of C_2D_2 gives rise to a similar overall pattern in the mid-IR, but due to the isotope shift, the ν_3 fundamental MVCD can be more easily measured, although a loss of S/N is still evident. The MVCD spectra of the $\nu_4 + \nu_5$ combination band and of the ν_3 fundamental band for C_2D_2 have also been measured. In general, negative MVCD A terms were observed for the ro-vibrational bands in these two MVCD spectra. The lower frequency half of the P branch of the ν_3 fundamental band suffers from interference due to residual CO_2 gas in our spectrometer; furthermore, two weaker hot bands, $\nu_4 \rightarrow \nu_3 + \nu_4$ and $\nu_5 \rightarrow \nu_3 + \nu_5$, overlap most of the ν_3 structure. In the mid-IR, the $\nu_4 + \nu_5$ combination band (band origin at about 1041.5 cm^{-1}) is overlapped by the $2\nu_4$ overtone band of C_2HD (band origin at about 1033.9 cm^{-1}). A part of the P branch for the $\nu_4 + \nu_5$ combination band of C_2D_2 is expanded and shown in Fig. 3 to illustrate how we were able to separate out the contributions from these two molecules and their different modes which happen

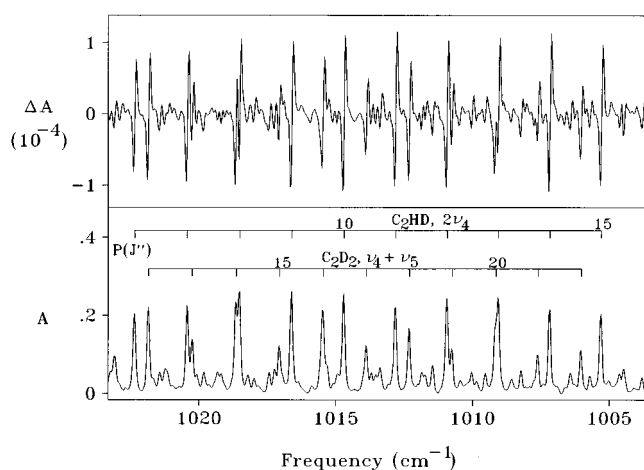


FIG. 3. The expansion of a part of the overlapped P branches of the $\nu_4 + \nu_5$ combination band of C_2D_2 and the $2\nu_4$ overtone band of C_2HD .

to be of similar intensity in this same sample. Despite this overlap of features from these two P branches, the same type of overall intensity variation is seen for this C_2D_2 combination band as in the MVCD spectrum of the $\nu_4 + \nu_5$ combination band of C_2H_2 . By comparison, the MVCD spectrum of the ν_3 fundamental band of C_2D_2 (with the exception of the CO_2 overlap region) has much more symmetrical relationship between the P - and R -branch contours, which indicates that the g_J -value in the ground and the ν_3 excited vibrational state are virtually equal.

The ro-vibrational bands for C_2H_2 are relatively well resolved which aids carrying out moment analyses on isolated transitions, but those for C_2D_2 are less resolved due to the smaller rotational constant for the deuterated isotopomer. Nevertheless, there are some isolated ro-vibrational transitions in C_2D_2 for which moment analysis can be effectively carried out. The signal-to-noise ratio (S/N) for the $\nu_4 + \nu_5$ spectrum of C_2D_2 is worse than that of C_2H_2 because of the lower absorbance level and smaller rotational magnetic moment for C_2D_2 . The S/N for the ν_3 spectrum of C_2D_2 is even worse due to the lower response of our rapid-scan spectrometer for higher frequencies. Since the rotational magnetic moment for acetylene is roughly an order of magnitude smaller than those of our previously studied molecules such as NH_3 , HCl , CH_4 , and CO ,^{6,14,16,17,24} the absolute MVCD signal intensities reported here are also small. Upgrading our spectrometer from its previous resolution of 0.5 to 0.1 cm^{-1} enhanced the MVCD signal level in these instrument resolution limited spectra. However, the noise level also increased due to the greatly increased scan time needed for 0.1 cm^{-1} resolution which consequently restricts the level of coaddition that is practical using our current interferometer design.

C. Moment analysis

The effective g_J values for all isolated transitions were extracted using moment analysis.³¹ First, the absorption and the MVCD spectra were fit with optimized mixtures of Lorentzian and Gaussian band shapes to reduce noise contri-

butions to the band shape integrals, particularly from baseline fluctuations.^{16,17} The values of these moments of each transition line shape were then evaluated by numerical integration of the fit curves. The A_1/D_0 parameter, which characterizes the magnitude and sign of the MVCD A term normalized by the absorbance, is given by³¹

$$\frac{A_1}{D_0} = \frac{\langle \Delta A \rangle_1}{\langle A \rangle_0} \frac{1}{B\beta}, \quad (15)$$

where B is the magnetic field strength and β is the Bohr magneton. $\langle A \rangle_0$ and $\langle \Delta A \rangle_1$, the zeroth moment of the absorbance and the first moment of the MVCD, respectively, are defined as follows:

$$\langle A \rangle_0 = \int \frac{A}{\nu} d\nu \quad \text{and} \quad \langle \Delta A \rangle_1 = \int \frac{\Delta A}{\nu} (\nu - \nu_c) d\nu, \quad (16)$$

where the center frequency, ν_c , is calculated by setting $\langle \Delta A \rangle_1 = 0$.

By the use of the above method, A_1/D_0 values for each ro-vibrational transition can be evaluated. In principle, it is also possible to analyze partially overlapped bands, but due to the large errors that resulted from attempting to curve fit the heavily overlapped bands, only A_1/D_0 values for the better isolated bands are reported. The results of moment analysis for the $\nu_4 + \nu_5$ combination of C_2H_2 are summarized in Table I. The results for the $R(10)$ to $R(18)$ transitions of the $\nu_4 + \nu_5$ combination band are missing due to their virtually zero MVCD intensity. Since the two hot bands, $\nu_4 \rightarrow 2\nu_4 + \nu_5$ and $\nu_5 \rightarrow \nu_4 + 2\nu_5$, have much lower absorption intensities than the $\nu_4 + \nu_5$ combination band, only some of the P -branch transitions can be adequately isolated and analyzed. For C_2D_2 , the moment analysis results for the $\nu_4 + \nu_5$ combination and the ν_3 fundamental band are summarized in Table II. Due to the serious overlap of the $\nu_4 + \nu_5$ combination band of C_2D_2 and the $2\nu_4$ overtone band of C_2HD , there are only a few isolated transitions for which moment analysis can be carried out. The ν_3 fundamental band contains several isolated features in spite of the interference from the CO_2 ro-vibrational bands in the P branch, but the reliability of the A_1/D_0 values is seriously impacted by the low S/N level for this MVCD transition.

D. C_2HD

The MVCD spectra for the $\nu_4 + \nu_5$ combination band of C_2HD has the same intense P branch and weak R -branch pattern as seen for this band in the other isotopomers, as shown in Fig. 4. Since C_2HD belongs to the $C_{\infty v}$ point group while C_2H_2 and C_2D_2 belong to the $D_{\infty h}$ point group, some overtone bands become symmetry allowed and can have appreciable intensities. The $2\nu_4$ overtone band which overlaps with the $\nu_4 + \nu_5$ combination band of C_2D_2 has been noted above in Fig. 3. Similarly, the $2\nu_5$ overtone band of C_2HD (band origin at about 1342.2 cm^{-1}) is seriously overlapped by the $\nu_4 + \nu_5$ combination band of C_2H_2 (band origin at about 1328.1 cm^{-1}), an unavoidable impurity in our C_2HD sample. The overlapped P -branch transitions of the $2\nu_5$ over-

TABLE I. Moment analysis results of the $\nu_4 + \nu_5$ combination band of C_2H_2 .

$P(J'')$ $R(J'')$	ν (cm^{-1})	$\langle A \rangle_0$ ($\times 10^2$)	$\langle \Delta A \rangle_1^a$ ($\times 10^3$)	A_1/D_0 ($\times 10^4$)	g_{eff}^b (n.m.)	$g_{eff}(\text{sim})^c$ (n.m)
$P(1)$	1325.72	6.02	-1.49	-0.531	+0.0487	+0.04903
$P(2)$	1323.37	4.12	-0.988	-0.513	+0.0471	+0.05246
$P(3)$	1321.03	9.18	-3.32	-0.774	+0.0710	+0.05589
$P(4)$	1318.70	7.27	-2.44	-0.717	+0.0658	+0.05933
$P(5)$	1316.38	11.9	-3.99	-0.719	+0.0660	+0.06276
$P(6)$	1314.06	7.16	-1.80	-0.537	+0.0493	+0.06619
$P(7)$	1311.75	14.3	-4.56	-0.681	+0.0625	+0.06962
$P(12)$	1300.31	8.29	-3.51	-0.907	+0.0833	+0.08678
$P(13)$	1298.05	17.1	-6.86	-0.859	+0.0789	+0.09022
$P(15)$	1293.51	13.7	-7.47	-1.17	+0.107	+0.09708
$P(16)$	1291.25	6.38	-3.32	-1.2	+0.102	+0.1005
$P(17)$	1288.99	9.38	-5.56	-1.27	+0.117	+0.1039
$P(18)$	1286.74	4.91	-2.78	-1.21	+0.111	+0.1074
$P(19)$	1284.50	8.60	-5.42	-1.35	+0.124	+0.1108
$P(22)$	1277.75	2.89	-1.87	-1.38	+0.127	+0.1211
$P(23)$	1275.50	3.71	-1.73	-1.00	+0.092	+0.1245
$P(24)$	1273.25	1.64	-0.964	-1.26	+0.116	+0.1280
$P(25)$	1270.99	2.63	-1.34	-1.09	+0.100	+0.1314
$P(26)$	1268.75	0.952	-0.618	-1.39	+0.128	+0.1348
$P(27)$	1266.49	1.84	-0.960	-1.12	+0.103	+0.1383
$P(28)$	1264.23	0.593	-0.285	-1.03	+0.0945	+0.1417
$P(29)$	1261.96	1.04	-0.584	-1.21	+0.111	+0.1451
$P(31)$	1257.42	0.607	-0.369	-1.30	+0.120	+0.1520
$R(0)$	1330.43	3.81	-0.766	-0.431	+0.0396	+0.04217
$R(1)$	1332.80	7.51	-1.82	-0.519	+0.0477	+0.03873
$R(2)$	1335.18	5.93	-1.42	-0.511	+0.0470	+0.03530
$R(3)$	1337.56	10.8	-1.98	-0.393	+0.0361	+0.03187
$R(4)$	1339.95	8.43	-1.12	-0.284	+0.0261	+0.02844
$R(5)$	1342.35	10.8	-2.01	-3.97	+0.0365	+0.02501
$R(6)$	1344.75	4.67	-0.821	-0.376	+0.0346	+0.02157
$R(9)$	1352.00	15.9	-1.19	-0.160	+0.0146	+0.01128
$R(19)$	1376.38	6.35	+0.240	+0.0809	-0.00742	-0.02304
$R(20)$	1378.82	3.13	+0.310	+0.212	-0.0195	-0.02648
$R(21)$	1381.26	5.07	+0.367	+0.155	-0.0143	-0.02991
$R(22)$	1383.70	1.81	+0.300	+0.354	-0.0325	-0.03334
$R(23)$	1386.13	3.28	+0.393	+0.257	-0.0236	-0.03677
$R(25)$	1390.98	2.30	+0.479	+0.446	-0.0409	-0.04364

^aIn units of cm^{-1} .^bIn terms of nuclear magneton.^c g_{eff} value derived from the simulated MVCD and IR absorption spectra with the rotational g value in the excited vibrational state being 14% less than the ground state g value.

tone band of C_2HD and the $\nu_4 + \nu_5$ combination band of C_2H_2 all have A_1/D_0 values corresponding to a positive rotational g value as illustrated for part of the P branch in Fig. 5. To correct for the latter interference from C_2H_2 , the absorption and MVCD spectra of the pure $\nu_4 + \nu_5$ combination band of C_2H_2 were subtracted from the C_2HD spectra using a single coefficient chosen to minimize the C_2H_2 absorbance contribution. Despite optimization, some residual spectral features from the $\nu_4 + \nu_5$ combination band of C_2H_2 are still present. In general, only negative MVCD A terms are observed in these MVCD spectra. For all three combination and overtone bands, we see an MVCD intensity variation similar to that which was observed in the $\nu_4 + \nu_5$ combination band of C_2H_2 . However, for the ν_3 fundamental band of C_2HD , as shown in Fig. 6, the MVCD intensities in the P and R branches are about the same, all having negative A terms,

which is consistent in terms of sign and band contour with the MVCD discussed above for the ν_3 band of C_2D_2 .

The MVCD spectra of the $\nu_4 + \nu_5$ and $2\nu_5$ bands of C_2HD (once corrected by subtraction of the $\nu_4 + \nu_5$ band of C_2H_2) are relatively free of interference, though there are other weak combination and hot bands underneath them. At the high J'' end of the R branch for the $\nu_4 + \nu_5$ band of C_2HD , there is some overlap with the tail of the P branch of the $\nu_4 + \nu_5$ band of C_2H_2 . The S/N of these C_2HD combination and overtone spectra are comparable and better than that attainable for the C_2D_2 spectra because of the higher absorbance levels that were possible under our sampling conditions. However, the S/N of the ν_3 band is again lower than for the mid-IR transitions due to the lower response of our spectrometer in rapid scan mode at higher optical frequencies.^{22,24}

TABLE II. Moment analysis summary of the $\nu_4 + \nu_5$ combination and the ν_3 fundamental bands of C_2D_2 .

$\nu_4 + \nu_5$			ν_3		
$P(J'')$	ν (cm^{-1})	g_{eff}^a (n.m.)	$P(J'')$ $R(J'')$	ν (cm^{-1})	g_{eff}^a (n.m.)
$P(4)$	1034.75	+0.0562	$P(3)$	2434.29	+0.0325
$P(6)$	1031.43	+0.0475	$P(5)$	2430.87	+0.0373
$P(7)$	1029.97	+0.0359	$P(6)$	2429.12	+0.0418
$P(8)$	1028.15	+0.0337	$P(7)$	2427.38	+0.0299
$P(9)$	1026.52	+0.0603	$P(8)$	2425.62	+0.0307
$P(10)$	1024.90	+0.0677			
$P(11)$	1023.29	+0.0741	$R(10)$	2457.49	+0.0316
$P(12)$	1021.68	+0.0623	$R(13)$	2462.23	+0.0397
			$R(14)$	2463.78	+0.0393
			$R(15)$	2465.33	+0.0383
			$R(16)$	2466.87	+0.0343
			$R(18)$	2469.93	+0.0306
			$R(20)$	2472.95	+0.0457
			$R(24)$	2478.87	+0.0365
			$R(25)$	2480.32	+0.0341

^aIn terms of nuclear magneton.

As for the C_2H_2 and C_2D_2 cases, moment analyses have been carried out for all the C_2HD spectra. The results are summarized in Table III for the $\nu_4 + \nu_5$ and ν_3 bands. Most of the $\nu_4 + \nu_5$, $2\nu_4$ and $2\nu_5$ ro-vibrational transitions in the P branch are isolated, thus permitting a reasonable analysis, while the much lower MVCD intensities in the R -branch result in a S/N level that is too low for reliable results.

V. DISCUSSION

A. Ground state molecular g_J values

The g_{eff} values derived from the moment analysis for the ro-vibrational bands for C_2H_2 , C_2D_2 and C_2HD were included in the last columns of Tables I–III. For acetylene and its deuterated isotopomers, the sign of the molecular g_J values in all the vibrational states we studied here are confirmed

unambiguously to be *positive*. For C_2H_2 , within our experimental error, the magnitude of the molecular g_J value in the ground vibrational state is determined to be 0.0535(33) using Eq. (14) which is in good agreement with 0.049 03(4) by the earlier MBMR measurement.⁶ The wide variation in g_J values for individual transitions is due primarily to the S/N limitations, but extrapolation through a number of transitions effects an averaging and consequent improvement in error provided the model used is appropriate.

Since there are no previous experimental data for the molecular g_J values for both C_2HD and C_2D_2 , we can extrapolate the molecular g_J value for C_2HD and C_2D_2 from that of C_2H_2 for the ground vibrational states. Let us assume that the internuclear axis is the z axis. It is well known that the g_J values in the x axis can be expressed as a sum of nuclear and electronic contributions,³³

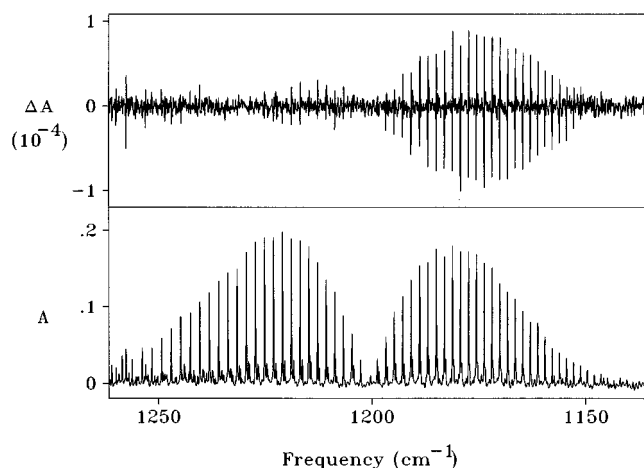


FIG. 4. The MVCD (upper) and IR absorption spectra (lower) of the $\nu_4 + \nu_5$ combination band of C_2HD . Resolution: 0.1 cm^{-1} ; MVCD shown is the difference of the MVCD measured in a field of $\pm 8\text{ T}$, each averaged over four blocks of 1024 scans.

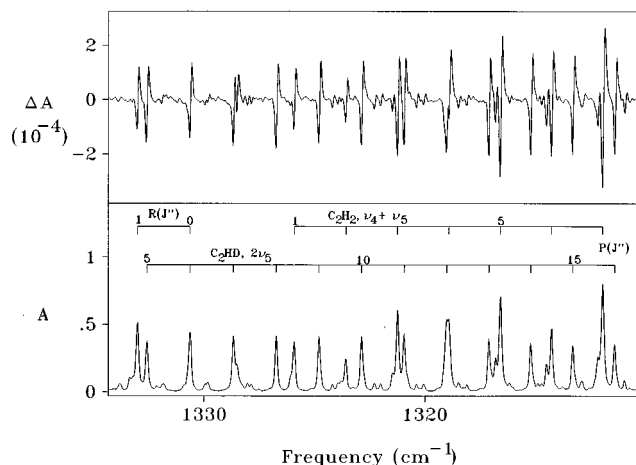


FIG. 5. The expansion of a part of the overlapped P branches of the $2\nu_5$ overtone band of C_2HD and the $\nu_4 + \nu_5$ combination band of C_2H_2 .

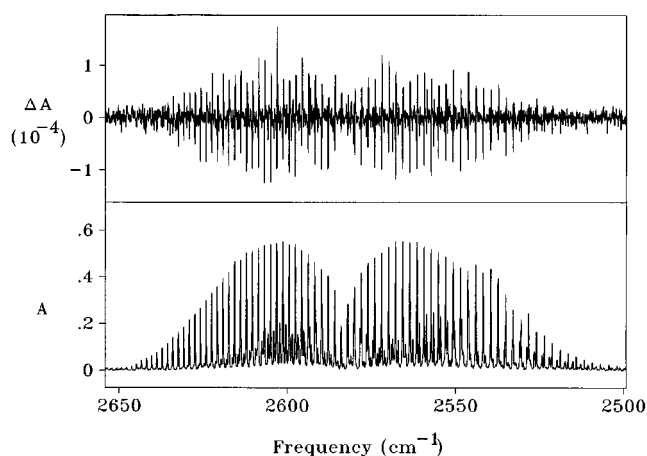


FIG. 6. The MVCD (upper) and IR absorption spectra (lower) of the ν_3 fundamental band of C_2HD . Resolution: 0.1 cm^{-1} ; MVCD shown is the difference of the MVCD measured in a field of $\pm 8 \text{ T}$, normalized to 1.0 T, each averaged over four blocks of 1024 scans.

$$g_{xx} = \frac{M_p}{I_{xx}} \sum_k Z_k z_k^2 - 2 \frac{M_p}{m I_{xx}} \sum_{n \neq 0} \frac{|\langle n | L_x | 0 \rangle|^2}{E_n - E_0}, \quad (17)$$

where M_p is the mass of a proton, I_{xx} is the moment of inertia, m is the mass of an electron, k sums over all nuclei, Z_k is the nuclear charge of the k th atom, z_k are the distances of the k th atom from the center of mass along the molecular

or z axis, and $\sum_{n \neq 0} |\langle n | L_x | 0 \rangle|^2 / (E_n - E_0)$ is the electronic orbital angular momentum contribution. By assuming that the bond lengths and the electronic orbital angular momentum matrix element remain constant after the substitution of deuterium for hydrogen, the ground state g_J value of C_2D_2 and C_2HD are calculated to be $+0.03533$ and $+0.04447$, respectively, from Eq. (17) using the accurate g_J value for the ground state of C_2H_2 taken to be $+0.04903$.^{6,8} Since the relative position of the center of mass of C_2HD is different from that of C_2D_2 and C_2H_2 , the electronic contribution to the g_J value for C_2HD may also differ from C_2H_2 and C_2D_2 . Therefore, extrapolation from the C_2H_2 g value may only give an approximate estimation of the ground state g_J values for C_2HD .

From analysis of the C_2D_2 MVCD using Eq. (14), the g_J value in the ground vibrational state is indicated to be $+0.0374(191)$ and $+0.0363(48)$ from the $\nu_4 + \nu_5$ and ν_3 band, respectively, which are in good agreement with each other and with the values extrapolated from C_2H_2 . However, the MVCD g_J value in the ground vibrational state for C_2HD is $+0.0336(68)$ from the $2\nu_5$ band, but is $+0.0493(122)$ from the $2\nu_4$ band, $+0.0349(126)$ from the $\nu_4 + \nu_5$ band and $+0.0409(69)$ from the ν_3 band. There is a much larger statistical variance in these C_2HD values between themselves and from the expected value than seen in the other two isotomers. Nevertheless, the experimental and calculated g_J

TABLE III. Moment analysis summary of the $\nu_4 + \nu_5$ combination and the ν_3 fundamental bands of C_2HD .

$\nu_4 + \nu_5$			ν_3		
$P(J'')$	ν	g_{eff}^a	$P(J'')$	ν	g_{eff}^a
$R(J'')$	(cm^{-1})	(n.m.)	$R(J'')$	(cm^{-1})	(n.m.)
$P(3)$	1194.59	+0.0253	$P(6)$	2571.72	+0.0322
$P(4)$	1192.63	+0.0369	$P(7)$	2567.66	+0.0411
$P(5)$	1190.68	+0.0387	$P(8)$	2567.58	+0.0435
$P(6)$	1188.73	+0.0375	$P(9)$	2565.49	+0.0556
$P(7)$	1186.80	+0.0480	$P(12)$	2559.14	+0.0349
$P(8)$	1184.88	+0.0463	$P(13)$	2557.00	+0.0382
$P(9)$	1182.97	+0.0484	$P(14)$	2554.85	+0.0303
$P(10)$	1181.06	+0.0508	$P(15)$	2552.68	+0.0313
$P(11)$	1179.18	+0.0470	$P(19)$	2543.83	+0.0483
$P(12)$	1177.30	+0.0695	$P(20)$	2541.62	+0.0442
$P(13)$	1175.43	+0.0474	$P(21)$	2539.41	+0.0383
$P(14)$	1173.58	+0.100			
$P(15)$	1171.74	+0.0670	$R(8)$	2597.32	+0.0335
$P(16)$	1169.92	+0.0699	$R(9)$	2599.20	+0.0422
$P(17)$	1168.12	+0.0979	$R(10)$	2601.06	+0.0332
$P(18)$	1166.33	+0.0531	$R(11)$	2602.91	+0.0484
$P(19)$	1164.56	+0.122	$R(12)$	2604.75	+0.0321
$P(20)$	1162.80	+0.157	$R(13)$	2606.57	+0.0364
$P(21)$	1161.07	+0.0830	$R(15)$	2610.17	+0.0392
$P(22)$	1159.36	+0.0815	$R(17)$	2613.66	+0.0356
			$R(18)$	2615.40	+0.0440
$R(7)$	1216.68	+0.0394	$R(19)$	2617.14	+0.0428
$R(8)$	1218.74	+0.0256	$R(20)$	2618.86	+0.0408
			$R(22)$	2622.28	+0.0500
			$R(25)$	2627.28	+0.0500
			$R(26)$	2628.92	+0.0338
			$R(27)$	2630.55	+0.0427

^aIn terms of nuclear magneton.

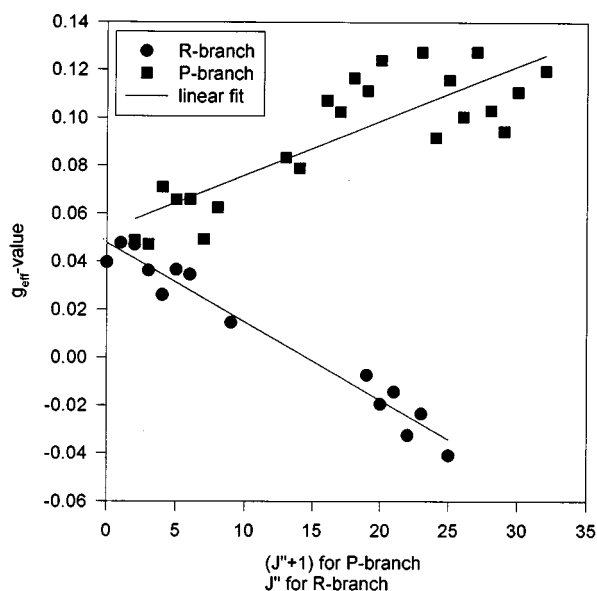


FIG. 7. The plot of g_{eff} values against $(J''+1)$ and J'' for the P and R branches, respectively, for the $\nu_4 + \nu_5$ combination band of C_2H_2 . The two straight lines are the results of linear regression for data in the P and R branches individually.

values for C_2HD are in reasonable agreement within their errors.

B. Excited state g_J values

The g_{eff} values for the ro-vibrational transitions involving ν_4 and ν_5 bending modes have a clear dependence on J . These g_{eff} values increase with J'' in the P branch and decrease with J'' in the R branch. However, the g_{eff} values for the ν_3 bands of C_2HD and C_2D_2 do not show a J dependence in either the P or R branches. The variation of these g_{eff}

values with J for the ν_3 bands are attributable to the random error of the intensity measurement. Thus acetylene in the bending combination modes offers the first example we have found for a large change (i.e., MVCD detectable) in the molecular g value for the excited nondegenerate vibrational states.

Figure 7 shows the plot of g_{eff} values against $J''+1$ and J'' for the P and R branches, respectively, of the $\nu_4 + \nu_5$ band of C_2H_2 . Two straight lines of oppositely signed slopes are obtained which fit the functionality of our model very well. From the slope and intercept, using Eq. (14), the molecular g_J values for the ground as well as the $\nu_4 + \nu_5$ excited vibrational level can be evaluated. The error of the MVCD derived g_J values were determined by a weighted linear least-squares fit using the first moment of the MVCD A term, $\langle \Delta A \rangle_1$, as the weight for each ro-vibrational transition. The excited state g -value results for all the transitions observed are summarized in Table IV. The slopes and hence Δg values for the $\nu_4 + \nu_5$ combination bands for the three isotopomers are all very similar. This is somewhat surprising in light of the substantial change in the ground state g value seen on deuteration in our MVCD results. On the other hand, for the ν_3 C–D stretching modes of C_2HD and C_2D_2 , the slopes for the plots of the g_{eff} values against J'' were at least a order of magnitude smaller than for the bending combination modes. Thus, within our detection capabilities, $g_{v'} = g_{v''}$ for the stretching modes.¹⁸

The standard deviations for the MVCD derived g -values for the $\nu_4 + \nu_5$ combination band of C_2H_2 (under 10%) are the smallest and the most reliable among the whole data set reported here (correlation coefficient of 0.94). Thus, the dependence of the g_{eff} values on J'' is statistically proven to be linear at a confidence level of 99%. However, the statistical variances for the two hot bands of C_2H_2 are large because of their low S/N and the smaller number of data points.

TABLE IV. The molecular g_J values of C_2H_2 , C_2HD , and C_2D_2 in the ground and various excited vibrational states as derived from MVCD.

Molecule	Lower vibrational state	Upper vibrational state	$g_{v''}^a$	$g_{v'}^b$	Δg^c
C_2H_2	Ground	$\nu_4 + \nu_5$	+0.0535 (33)	+0.0474 (29)	-0.0061 (4) ^d
	ν_4	$2\nu_4 + \nu_5$	+0.0488 (95)	+0.0428 (82)	-0.0060 (13)
	ν_5	$\nu_4 + 2\nu_5$	+0.0420 (204)	+0.0334 (179)	-0.0086 (25)
C_2HD	Ground	$\nu_4 + \nu_5$	+0.0349 (126)	+0.0283 (111)	-0.0066 (15)
	Ground	$2\nu_4^e$	+0.0493 (122)	+0.0464 (107)	-0.0029 (15)
	Ground	$2\nu_5^f$	+0.0336 (68)	+0.0262 (60)	-0.0074 (8)
	Ground	ν_3	+0.0409 (69)	+0.0409 (69)	0 ^e
C_2D_2	Ground	$\nu_4 + \nu_5^f$	+0.0374 (191)	+0.0322 (160)	-0.0052 (31)
	Ground	ν_3	+0.0363 (48)	+0.0363 (48)	0 ^e

^aMolecular g_J value in the lower vibrational state.

^bMolecular g_J value in the upper vibrational state.

^c Δg is calculated from $g_{v'} - g_{v''}$.

^dThe parentheses indicate the error, for example, $-0.0061(4) = -0.0061 \pm 0.0004$.

^eThe slope obtained from the linear regression of the data for the C–D stretching modes as well as the correlation coefficients of the linear fits are negligibly small. Therefore we assume the slope or Δg are zero for these C–D stretching bands.

^fThe $2\nu_4$ band of C_2HD overlaps with the $\nu_4 + \nu_5$ band of C_2D_2 (see Fig. 3); the $2\nu_5$ band of C_2HD overlaps with the $\nu_4 + \nu_5$ band of C_2H_2 (see Fig. 5). That is why the g values derived from these overlapped bands of C_2HD and C_2D_2 have a larger variance than those from the other relatively isolated vibrational bands.

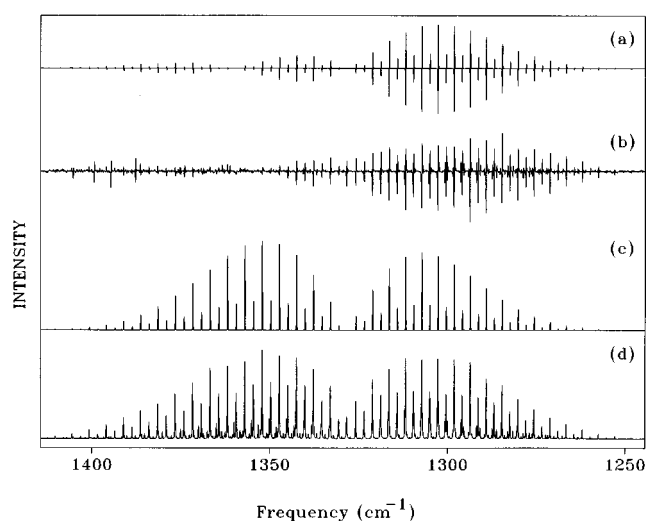


FIG. 8. The (a) simulated ($g_{v'}=0.86g_{v''}$) and (b) experimental MVCD spectra of the $\nu_4+\nu_5$ combination band of C_2H_2 , respectively; (c) and (d) are the corresponding absorbances.

On the other hand, the MVCD derived g values for the ν_3 C–D stretching bands for both C_2HD and C_2D_2 are also reasonably reliable having standard deviations equivalent to about 15%. There is a larger error for the $\nu_4+\nu_5$ band of C_2HD ($\sim 33\%$) which can be attributed to the limited S/N. However, the statistical errors for the MVCD derived g values for the $2\nu_4$ of C_2HD and the $\nu_4+\nu_5$ combination band of C_2D_2 are worse (and correlation coefficients are smaller) because of the heavy overlap between the $2\nu_4$ band of C_2HD and the $\nu_4+\nu_5$ band of C_2D_2 (see Fig. 3). In all cases, these excitations of bending motion yield reduced excited state g values as is clearly evident from their ro-vibrational MVCD band profiles. Even for the hot combination bands, $\nu_4\rightarrow 2\nu_4+\nu_5$ and $\nu_5\rightarrow \nu_4+2\nu_5$, seen in C_2H_2 , which are $\pi_g\rightarrow(\Pi\pi_u)$ and $\pi_u\rightarrow(\Pi\pi_g)$ transitions⁴ have the same band profiles indicating a reduction in molecular g value with bending excitation.

Since the ν_3 stretching modes for C_2HD and C_2D_2 do not show this trend, indicating no decrease in g_J value for these modes, the negative Δg seen for the combination bands must be due to the change of the molecular symmetry on bending deformation. One possible explanation might be that the bending motions impose a perturbation on the π system of acetylene because the molecule is no longer perfectly linear. In addition, upon time averaging, the effective C–H bondlength along the $C\equiv C$ axis will be shorter in the excited bending levels than the ground state or in an excited stretching mode. This change in geometry will lower the nuclear contribution to the g_J value, thus causing the positive g_J value to decrease in the excited bending levels. As the amplitude of the bending motion increases, the electronic perturbation and the change in nuclear geometry will also be larger leading to a larger change in g_J value.

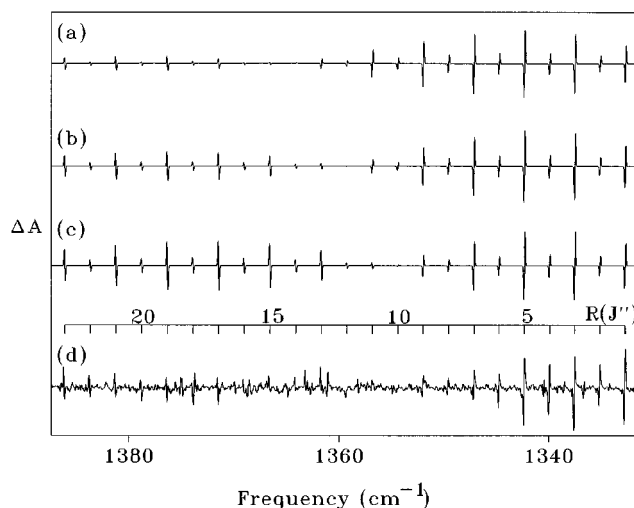


FIG. 9. The simulated MVCD spectrum of the $\nu_4+\nu_5$ combination band of C_2H_2 with the rotational g value in the excited vibrational state being (a) 12%, (b) 14%, (c) 16%, smaller than the ground state g value and (d) the corresponding experimental MVCD spectrum.

C. Theoretical simulation for the C_2H_2 $\nu_4+\nu_5$ combination band

As an alternative analysis of the $g_{v'}\neq g_{v''}$ observation, we have simulated the IR absorption and MVCD spectra of the $\nu_4+\nu_5$ band of C_2H_2 . We selected this vibrational band because its spectra have the best S/N among those in the data set available for this study.

The theory on which this simulation is based has been described in Sec. III. Pliva's set of molecular constants³ was used to construct the energy matrix with the addition of several up-dated constants.²⁹ The g_J value in the ground was taken to be +0.049 03 (Refs. 6 and 8) and then the excited g_J value was varied to obtain the best agreement between the simulated and the experimental MVCD spectra. The intensity of the absorption and MVCD spectra were calculated as $(A_-+A_+)/2$ and $(A_- - A_+)$, respectively using Eq. (11), summing over all $|JM\rangle$ states and imposing a realistic band shape upon the results. This simulation was carried out using an Ardent Titan workstation with programs written in house.

Figure 8 shows the overall simulated ($g_{v'}=0.86g_{v''}$) and experimental MVCD and IR absorption spectra of the $\nu_4+\nu_5$ band of C_2H_2 . In general, the qualitative agreement is excellent. The MVCD intensity variation between the P and R branches are very similar for both the simulated and experimental MVCD spectra. However, as we have seen in our previous simulations of DC1 and NH_3 MVCD and absorption spectra, the shape of the rotational envelope is distorted (flattened) in the experimental data as compared to the simulation. In addition, the intensity variation with nuclear spin is not as sharp as expected from theory. Both of these effects are probably due in part to photometric inaccuracy of our FTIR instrument for bands that are totally instrument line-width limited. Ratioing the moments of the simulated spectra to derive A_1/D_0 for these bands does yield better agreement as shown in the last column of Table I where the trend in g_{eff} and $g_{\text{eff}}(\text{sim})$ show an excellent match indicating that we

now properly understand this MVCD spectrum.

Figures 9(a)–9(c) show a part of the R branch of the simulated MVCD spectra of the $\nu_4 + \nu_5$ band of C_2H_2 that was simulated using an excited vibrational state g_J value 12%, 14%, and 16% smaller than the ground state g value, respectively. Figure 9(d) shows the corresponding experimental MVCD spectrum. By comparing the MVCD intensity envelopes and positions of sign change for individual rovibrational transitions of the simulated and experimental MVCD spectra, we feel that Fig. 9(b) matches the experimental spectrum the best. Exact comparison is impossible due to the S/N, so that the decrease in the $\nu_4 + \nu_5$ excited state g value determined from simulation should be considered to be $14 \pm 2\%$. Alternatively, from the plot of g_{eff} vs J'' in Fig. 7, it can be seen that the g_{eff} value crosses zero at about $J'' = 15$ in the R branch which is in reasonable agreement with the overall simulation shown in Fig. 8. These simulation results are consistent with the experimental $\Delta g = -0.0061$ value found above using Eq. (14).

VI. CONCLUSION

The molecular g_J values of C_2H_2 , C_2HD , and C_2D_2 in the ground and various excited vibrational states have been determined by MVCD measurements. The sign of all the underlying rotational g values is unambiguously *positive* for these molecules in all the modes studied. The apparent g_{eff} values do have a sharp J dependence which was used to determine the rotational g value for the excited states. The g values in the excited bending vibrational states of C_2H_2 , C_2HD , and C_2D_2 are all smaller than those in the ground vibrational states. In contrast, the g_J values in the excited stretching vibrational states are roughly equal to those in the ground vibrational state. These data clearly demonstrate changes in the g value upon bending vibrational excitation which appears to correlate with distortion of the linear molecule in those modes. Further, the theoretically simulated MVCD spectrum of the C_2H_2 $\nu_4 + \nu_5$ band best fits the experimental spectrum for an excited state rotational g value that is 14% smaller in magnitude than the ground state g -value. The excited state g value derived from simulation and from moment analyses of the experimental MVCD spectra are found to be in adequate agreement and clearly demonstrate the capability of MVCD to differentiate between excited state g values of sufficiently different magnitude.

ACKNOWLEDGMENTS

This research was supported in part by the National Science Foundation and by the University of Illinois through a

Senior Scholar Award (to T.A.K.) and a Dean's Scholar Fellowship (to C.N.T.). P.B. is supported by the Grant Agency of the Czech Republic (Grants 203/93/0714 and 203/95/0105). C.N.T. would also like to thank Mrs. Philip L. Hawley for the Philip L. Hawley Fellowship administered through the University of Illinois at Chicago.

- ¹G. Herzberg, *Molecular Spectra and Molecular Structure, II. Infrared and Raman Spectra of Polyatomic Molecules* (Van Nostrand, London, 1945).
- ²J. Pliva, *J. Mol. Spectrosc.* **44**, 145 (1972).
- ³J. Pliva, *J. Mol. Spectrosc.* **44**, 165 (1972).
- ⁴Y. Kabbadj, M. Herman, G. D. Lonardo, L. Fusina, and J. W. C. Johns, *J. Mol. Spectrosc.* **150**, 535 (1991).
- ⁵J. V. Auwera, D. Hurtmans, M. Carleer, and M. Herman, *J. Mol. Spectrosc.* **157**, 337 (1993).
- ⁶J. W. Cederberg, C. H. Anderson, and N. F. Ramsey, *Phys. Rev.* **136**, A960 (1964).
- ⁷S. L. Hartford, W. C. Allen, C. L. Norris, E. F. Pearson, and W. H. Flygare, *Chem. Phys. Lett.* **18**, 153 (1973).
- ⁸L. A. Cohen, J. H. Martin, and N. F. Ramsey, *Phys. Rev. A* **19**, 433 (1979).
- ⁹C. N. Tam and T. A. Keiderling, *Chem. Phys. Lett.* **243**, 55 (1995).
- ¹⁰T. A. Keiderling, *J. Chem. Phys.* **75**, 3639 (1981).
- ¹¹C. N. Tam, B. Wang, T. A. Keiderling, and W. G. Golden, *Chem. Phys. Lett.* **198**, 123 (1992).
- ¹²T. R. Devine and T. A. Keiderling, *J. Chem. Phys.* **83**, 3749 (1985).
- ¹³T. R. Devine and T. A. Keiderling, *J. Phys. Chem.* **88**, (1984).
- ¹⁴B. Wang, P. V. Croatto, R. K. Yoo, and T. A. Keiderling, *J. Phys. Chem.* **96**, 2422 (1992).
- ¹⁵B. Wang, R. K. Yoo, P. V. Croatto, and T. A. Keiderling, *Chem. Phys. Lett.* **180**, 339 (1991).
- ¹⁶B. Wang and T. A. Keiderling, *J. Chem. Phys.* **98**, 903 (1993).
- ¹⁷C. N. Tam and T. A. Keiderling, *J. Mol. Spectrosc.* **157**, 391 (1993).
- ¹⁸P. Bour, C. N. Tam, B. Wang, and T. A. Keiderling, *Mol. Phys.* (in press).
- ¹⁹T. A. Keiderling, in *Practical Fourier Transform Spectroscopy*, edited by K. Krishnan and J. R. Ferraro (Academic, San Diego, 1990), p. 203.
- ²⁰R. K. Yoo, P. V. Croatto, B. Wang, and T. A. Keiderling, *Appl. Spectrosc.* **45**, 231 (1990).
- ²¹B. Wang, Ph. D. Thesis, University of Illinois at Chicago, 1993.
- ²²B. Wang and T. A. Keiderling, *Appl. Spectrosc.* **49**, 1347 (1995).
- ²³C. N. Tam, Ph. D. Thesis, University of Illinois at Chicago, 1995.
- ²⁴B. Wang and T. A. Keiderling, *J. Phys. Chem.* **98**, 3957 (1994).
- ²⁵J. I. Steinfeld, *Molecules and Radiation*, 2nd ed. (MIT, Cambridge, MA, 1985).
- ²⁶A. Baldacci, S. Ghersetti, S. C. Hurlock, and K. N. Rao, *J. Mol. Spectrosc.* **59**, 116 (1976).
- ²⁷S. Ghersetti, J. Pliva, and K. N. Rao, *J. Mol. Spectrosc.* **38**, 53 (1971).
- ²⁸M. Herman, T. R. Huet, Y. Kabbadj, and J. V. Auwera, *Mol. Phys.* **72**, 75 (1991).
- ²⁹J. K. G. Watson, M. Herman, J. C. V. Craen, and R. Colin, *J. Mol. Spectrosc.* **95**, 101 (1982).
- ³⁰K. M. T. Yamada, F. W. Birss, and M. R. Aliev, *J. Mol. Spectrosc.* **112**, 347 (1985).
- ³¹P. J. Stephens, *Adv. Chem. Phys.* **35**, 197 (1976).
- ³²P. Bour, C. N. Tam, and T. A. Keiderling, *J. Phys. Chem.* (in press).
- ³³W. Gordy and R. L. Cook, *Microwave Molecular Spectra*, 3rd ed. (Wiley, New York, 1984).

The Journal of Chemical Physics is copyrighted by the American Institute of Physics (AIP). Redistribution of journal material is subject to the AIP online journal license and/or AIP copyright. For more information, see <http://ojps.aip.org/jcpo/jcpcr/jsp>
Copyright of Journal of Chemical Physics is the property of American Institute of Physics and its content may not be copied or emailed to multiple sites or posted to a listserv without the copyright holder's express written permission. However, users may print, download, or email articles for individual use.

The Journal of Chemical Physics is copyrighted by the American Institute of Physics (AIP). Redistribution of journal material is subject to the AIP online journal license and/or AIP copyright. For more information, see <http://ojps.aip.org/jcpo/jcpcr/jsp>